Volume 62
Number 21
17 March 2026
Pages 5769–5992

ChemComm

Chemical Communications

rsc.li/chemcomm

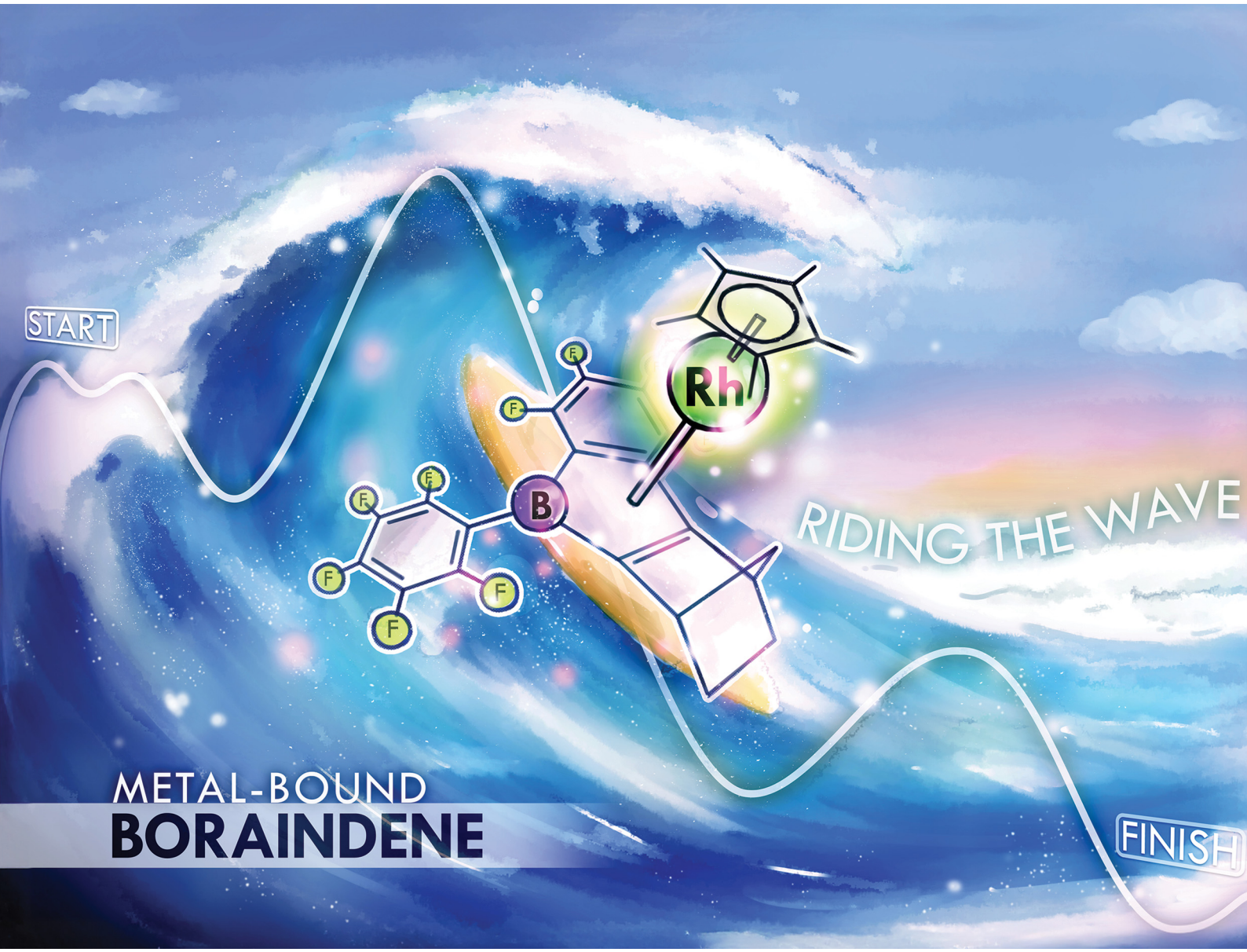

ISSN 1359-7345

ROYAL SOCIETY OF CHEMISTRY

COMMUNICATION

David J. Nelson, Marcus W. Drover *et al.*

From borane to metal-bound boraindene: a cascade of bond breaking and making at rhodium

ChemComm

COMMUNICATION

View Article Online
View Journal | View Issue

Cite this: *Chem. Commun.*, 2026, **62**, 5871

Received 8th January 2026,
Accepted 3rd February 2026

DOI: 10.1039/d6cc00158k

rsc.li/chemcomm

From borane to metal-bound boraindene: a cascade of bond breaking and making at rhodium

Emily J. Addison,[a] Joseph A. Zurakowski,[a] Paul D. Boyle,[a] David J. Nelson *[b] and Marcus W. Drover *[a]

Few monobenzannulated 1-boraindene compounds have been reported. Here we report the synthesis of two 1-boraindenes, accessed by a bond-breaking and -making cascade from a secondary borane and diolefin, mediated by a simple pentamethylcyclopentadienyl-ligated rhodium(I) complex, [(Cp*)Rh(η^2,η^2-NBD)] (Cp* = $C_5Me_5^-$, NBD = norbornadiene).

Main group heterocycles find diverse applications in medicine, catalysis, and materials sciences.[1] The introduction of heteroatoms into a cyclic core allows for compound tunability.[2] Heterocycles that include a group 13 element, for instance, provide a vacant p-orbital that extends π-conjugation and alters molecular properties.[3] Lewis acid incorporation additionally offers a site for Lewis base binding, providing an axis for tuned physical properties; this is notably absent for more canonical carbon- and nitrogen-based rings.

Resembling indole and its carbon analogue, indene, 1-boraindenes are fused six-five heterocycles featuring boron within the smaller C_4E ring (E = element). The electronic and structural properties of these compounds can be tuned by peripheral substitution. The chemistry of related six-five-six borafluorene analogues has been extensively explored,[4] but considerably less attention has been given to 1-boraindenes (*e.g.*, **I**, Fig. 1).[5,6] 1-Boraindenes display metallomimetic[7] reactivity, such as reversible addition of H_2 and cyclohexene hydrogenation.[6] They remain relatively neglected, as noted by Braunschweig, who in 2024 described only the second example (**II**, Fig. 1).[8,9] Developing creative and efficient synthetic routes to 1-boraindene cores is paramount to unlocking new applications. Related work on borafluorenes, for example,[4] showcases their broad utility as organic light-emitting diodes,[10] medical imaging agents,[11] sensors,[12] co-catalysts,[13] and bifunctional ligands (**III**, Fig. 1).[14,15]

Herein we share an unusual route towards the 1-boraindene core from a secondary borane and diolefin through a series of Rh-mediated C(sp^2)–F and C(sp^3)–H activations, C–C reductive elimination, and alkene dehydrogenation and hydrogenation. This complex transformation merges borane and olefin groups to give a rhodium-bound 1-boraindene heterocycle, highlighting the resourcefulness of [(Cp*)Rh^I], resulting in an unprecedented approach to 1-boraindene cores. This report serves as a rare opportunity to dissect and repurpose well-defined bond activation pathways such as olefin functionalization and reductive elimination processes at Rh to rationally prepare new main group heterocycles.

A yellow-orange C_6D_6 (or toluene) solution of [(Cp*)Rh^I(η^2,η^2-NBD)] (**1**) (Cp* = $C_5Me_5^-$, NBD = norbornadiene), treated with 1 equiv. $HB(C_6F_5)_2$ (Piers's borane) at 25 °C, changed color to dark red (Fig. 1). By ^{19}F NMR spectroscopy, $HB(C_6F_5)_2$ was consumed to produce several $-C_6F_x$ (x = 3–5) fragments. Following workup and extraction into pentane, this mixture consistently deposited red blocks that were suitable for single crystal X-ray diffraction analysis (25–30% isolated yield). The product, [Cp*Rh(1-boraindene-R)] (**2-R:** R = H or F), is an 18e$^-$ complex, comprising a core η^5-BC_4 ligand system that links norbornadiene and $HB(C_6F_5)_2$ units (Scheme 1). In one resonance contributor,

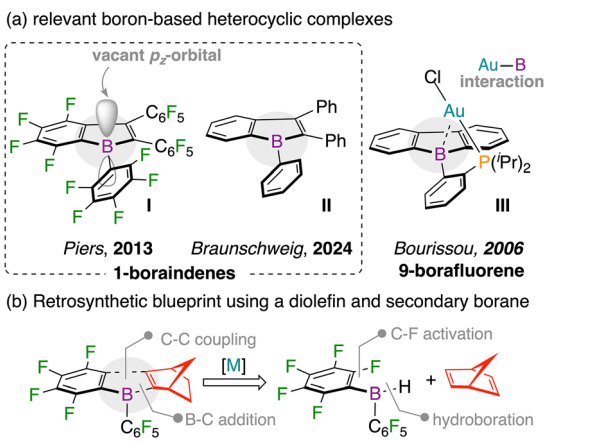

Fig. 1 (a) Boron heterocycles from the literature. (b) This work.

[a] *Department of Chemistry, Western University, 1151 Richmond Street, London, ON, N8K 3G6, Canada. E-mail: marcus.drover@uwo.ca*

[b] *Department of Pure and Applied Chemistry, University of Strathclyde, 295 Cathedral Street, Glasgow, G1 1XL, UK. E-mail: david.nelson@strath.ac.uk*

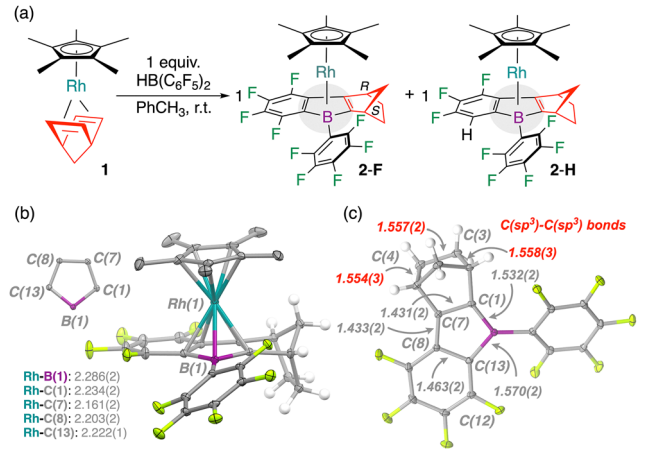

Scheme 1 (a) Synthesis of Cp*Rh-coordinated 1-boraindenes **2-H** and **2-F**; (b) Molecular structure of **2-H**/**2-F** with ellipsoids drawn at 40% probability. Major component: R = F shown only in both. A 60 : 40 substitutional disorder at C(12) was found for **2-H**/**2-F**. Hydrogen atoms, except those on the norbornene ring, omitted for clarity; (c) Top view, with Cp*Rh fragment omitted. Distances provided in Å.

these ligands can be considered dianionic 6π-electronic systems analogous to Cp containing a Rh(III) center.[16,17] By positive-mode APCI-MS, molecular ions ($[M]^+$) for **2-H** and **2-F** were observed at *m*/*z* = 638.089 (calc'd 638.090 for **2-H**) and *m*/*z* = 656.079 (calc'd 656.080 for **2-F**) of the appropriate isotope patterns. The transformation requires **1** – no reaction is observed using (*e.g.*) $[Rh^I(NBD)(\mu\text{-}Cl)]_2$. **2-R** are the first examples of 1-boraindene coordination complexes; a related phosphine-tethered borafluorene-Au analogue (**III**, Fig. 1) is known.[14,15] The formation of **2-F** formally involves the loss of one hydrogen and one fluorine atom, whereas the formation of **2-H** involves the loss of two fluorine atoms; **2-H** and **2-F** differ by H/F exchange at C(12) (*vide infra*). Although this cascade to give 1-boraindene products is unprecedented, the overall transformation of coupling a diene and *triaryl*borane to give a borole has some precedent using 1,3-butadiene and $B(C_6F_5)_3$ at zirconium to give [Cp′Zr(η^5-$C_4H_4BC_6F_5$)], from C–H activation.[18]

Structural analysis confirmed selective formation of the *exo*-product where [Cp*Rh^I] and the –CH_2– bridgehead occupy the same face (Rh. . .H(C){NBD} = *ca.* 3.01 Å) (Scheme 1(b) and (c)). **2-H** and **2-F** contain point chirality at both NBD methines and planar chirality arising from the linkage of the 1-boraindene and NBD rings. In principle, **2-R** could form multiple diastereomers but only one is observed experimentally. **2-H** and **2-F** contain a saturated external NBD fragment with d[C(3)-C(4)] = 1.557(2) Å *c.f.*, d[C(1)–C(7)] = 1.431(2) Å, evidencing formal transfer hydrogenation. With the B-(C_6F_5) group front-facing, the Cp*Rh fragment is rear-tilted with closer contacts to C(7) and C(8), when compared to C(1) and C(13). A Rh–B(1) distance of 2.286(2) Å is well within the sum of van der Waals radii (3.80 Å)[19] and close to the sum of covalent radii (2.26 Å).[20] These metrics can be compared to Rh–B(1) for related borole compounds [CpRh(η^5-C_4H_4BPh)][21,22] (2.304(4) Å) and [$Rh(PPh_3)_2(Cl)(\eta^5$-C_4H_4BPh)][23] (2.400(5) Å). The structures of **2-R** contain substitutional disorder, best modelled as a 60 : 40 split between C–H and C–F substituents at C(12), consistent with some C(12)-H/F exchange.[24,25] This points to activation of both *ortho* C–F bonds of the pentafluorophenyl ring: one undergoes C(sp^2)–F activation and C–C ring closure and another undergoes partial C(sp^2)–F/C(sp^2)–H exchange, presumably due to C–H reductive elimination.

Crystalline **2** was characterized in solution (see the SI). By ^{19}F NMR spectroscopy, the 17 fluorine atoms observed in the crude mixture were clearly identified. [^{19}F, ^{19}F] COSY attributed ten of these to two different B-C_6F_5 rings (*ca.* 1 : 1 ratio; multiplets at δ_F = −127.3/−127.4 (F_o), −156.8/−157.1 (F_p), and −163.7/−164.2 ppm (F_m)). The difference in peak separation between F_p and F_m ($\Delta\delta_F \approx 6$ ppm) suggests a four-coordinate borane,[26] also supported by ^{11}B NMR spectroscopy (δ_B = 4.6 ppm, $\Delta_{1/2}$ = 250 Hz). Based on scalar coupling, the remaining seven fluorines comprise –C_6F_4 and –C_6F_3H rings. ^{19}F{^{1}H} NMR spectroscopy shows the latter coupling to an adjacent C(sp^2)–H, as supported by the solid-state structure of **2-H**. The presence of two 1-boraindene molecules is corroborated by ^{1}H NMR spectroscopy, which shows the expected norbornyl-derived aliphatic signals and two sets of Cp*(CH_3) signals (δ_H = 1.25/1.21 ppm) in a 1 : 1 ratio. A characteristic resonance at δ_H = 6.88 ppm shows coupling to three fluorine atoms ($^3J_{H,F}$ = 11.2, $^4J_{H,F}$ = 7.0, $^5J_{H,F}$ = 1.5 Hz) that is removed during ^{19}F{^{1}H} NMR analysis of the –C_6F_3H ring.

The reaction between **1** and $HB(C_6F_5)_2$ was repeated at −78 °C (for 30 min) and then warmed to room temperature. Analysis by ^{19}F{^{1}H} NMR spectroscopy revealed that **2-H** was not formed (Fig. S16), suggesting that **2-F** is the kinetic product, while **2-H** arises from a distinct, higher-energy pathway, possibly after HF elimination. This demonstrates that formation of **2-F** is viable under these conditions, with the reaction likely proceeding upon warming to room temperature.

To gain further insight into this reaction we used DFT calculations at the r^{2}SCAN0-D4[27,28]/MA-Def2-QZVP[29]/SMD (toluene)[30]//r^{2}SCAN-3c[31] level of theory (with ORCA).[32,33] Full details are in the Supporting Information. Free energies are quoted in kcal mol^{-1}, relative to **1** and $HB(C_6F_5)_2$ and include a 1.89 kcal mol^{-1} per molecule correction to reflect a 1 mol L^{-1} concentration.[34] Transition state (TS) images were prepared using CYLView.[35]

A natural localized molecular orbital (NLMO) analysis of **2-F** (NBO7)[36] reveals the nature of the bonding between rhodium and the 1-boraindene fragment (Fig. 2). Visualization of the NLMOs with ChemCraft[37] identified occupied NLMOs 077 and 083 that each result from mixing of a Rh d_{xz} or d_{yz} orbital with a p-orbital on a C atom of the alkene. Unoccupied NLMOs 154 and 160 are consistent with an antibonding interaction between the Rh d-orbitals and the C p-orbitals. Finally, unoccupied NLMOs 227 and 228 indicate antibonding interactions between the B p-orbital and C p-orbitals, with antibonding interactions with Rh in each case.

A proposed mechanism accounting for the formation of **2-F** from **1** and [Cp*Rh(NBD)] was explored by DFT. While several pathways were identified, high computed barriers preclude definitive conclusions regarding the operative mechanism at this stage (Fig. S33 and S34, see SI). We therefore provide only a summary of the processes considered here, with a full discussion in the SI. Our

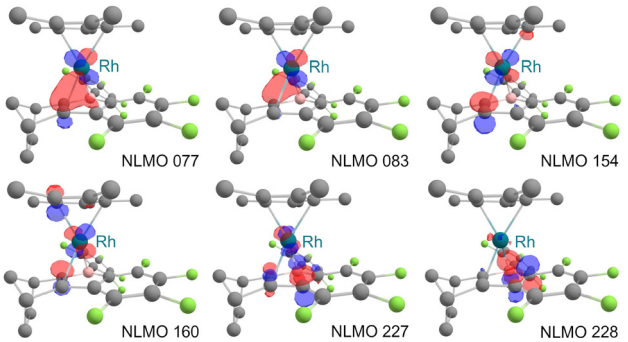

Fig. 2 Visualization of selected NLMOs for **2-F**: NLMO 077 (occupied), NLMO 083 (occupied), NLMO 154 (unoccupied), NLMO 160 (unoccupied), NLMO 227 (unoccupied), and NLMO 228 (unoccupied).

investigation first considered hydroboration between NBD and $HB(C_6F_5)_2$, which undergo a known *exo*-selective reaction[38–40] at room temperature in the absence of a catalyst to give **3** (see the SI). Subsequent steps considered include ortho-C–F bond activation, a series of C–H bond activations, and scaffold rearrangement leading to formation of a new C–C bond *via* reductive elimination. Finally, a hydrogenation/dehydrogenation sequence was examined to account for formation of the observed product, **2-F**. The key issues at this stage are around the timing and mechanism of HF elimination, which is difficult to track experimentally; the two emerging pathways involve either: (i) HF elimination at an early stage, therefore requiring a challenging C-C reductive elimination from rhodium(III), or (ii) a more facile reductive elimination from rhodium(V) but which then leads to highly stable intermediates that will not readily eliminate HF.

Additional control experiments were next conducted. Consistent with the calculated free energy difference between **1** + $HB(C_6F_5)_2$ and its *exo*-hydroboration product (7.8 kcal mol^{-1}), no stoichiometric exchange is observed between **1** and *exo*-**3** (prepared *via* NBD hydroboration with 1 equiv. $HB(C_6F_5)_2$)[41,42] (Fig. 3a), consistent with the calculated equilibrium constant (1.9×10^{-6}).

It is likely that during the formation of **2-F**, HF is expelled where the 'H' is $HB(C_6F_5)_2$-derived. To experimentally probe this, $[DB(C_6F_5)_2]_2$ was used, giving a 1 : 3 ratio of **2-H** to **2-F** (*c.f.* 1 : 1 from $[HB(C_6F_5)_2]_2$). APCI-HRMS afforded an isotopic distribution envelope for **2-H** and **2-F** (Fig. S29 and S30). Unlike the spectrum of **2-H** and **2-F** generated from $[HB(C_6F_5)_2]_2$ (single isotopologues), the spectrum from the $[DB(C_6F_5)_2]_2$ reaction was best modeled as a 60 : 40 ratio of **2-H-d_0** to **2-H-d_1**, and a 50 : 50 ratio of **2-F-d_0** to **2-F-d_1** (Fig. 3(b)). ^{1}H NMR spectroscopy indicated no evidence of C(sp^2)–D or methine C–D, but ^{2}H NMR spectroscopy showed deuterium in the $-CH_2$-CH_2- fragment (Fig. S24 and S25). This suggests that both β-*syn* and β-*anti* C–H activation pathways operate, and that HF elimination is not product-determining. TSs for *syn* (**TS-EF**) and *anti* C-H activation (*anti*-**TS-EF**) were examined for the d_0 and d_1 isotopologues, as outlined in the Supporting Information. For the d_0 substrate, **TS-EF** is 1.9 kcal mol^{-1} lower in energy than *anti*-**TS-EF**; in the case of the d_1 substrate, *anti*-**TS-EF** is 0.3 kcal mol^{-1} lower in energy. These free energy differences are around the limits of DFT accuracy, but the trend suggests that selective

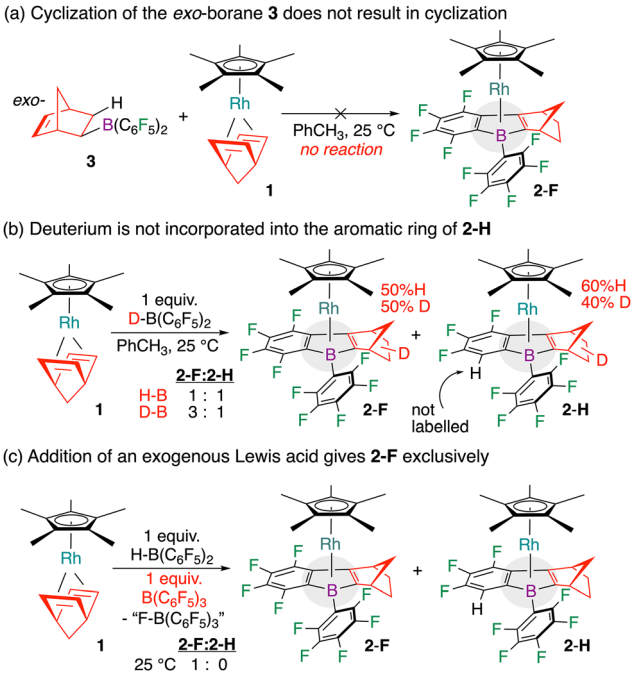

Fig. 3 Probing the mechanism for generation of **2-H**/**2-F**.

deuteration of the hydroborated norbornadiene changes subsequent C–H activation selectivity.

2-F does not convert into **2-H** in solution, even in the presence of excess $HB(C_6F_5)_2$ or $B(C_6F_5)_3$, but trace $B(C_6F_5)_3$ - used in the preparation of $HB(C_6F_5)_2$ – alters the product distribution in favour of **2-F** in the reaction between **1** and $HB(C_6F_5)_2$; a reaction in the presence of 1 equiv. $B(C_6F_5)_3$ in C_6D_6 at 25 °C afforded only **2-F** (Fig. S24 and Fig. 3(c)). A new broad resonance at $\delta_F = -188$ ppm was assigned to the formation of a species such as $[FB(C_6F_5)_3]^-$[43] which might arise from $B(C_6F_5)_3$ trapping HF to give $(HF)_nB(C_6F_5)_3$,[44] which decomposes to yield fluoroborate. Use of excess $HB(C_6F_5)_2$ (5 equiv.) also supresses **2-H** formation, giving **2-H** and **2-F** in a 1 : 4 ratio. These observations support a mechanism in which HF elimination precedes **2-H** formation.

In sum, we have presented a unique approach towards an understudied class of borane-based heterocycle by taking advantage of a diolefin/secondary borane coupling strategy at Rh(I). A new complex **2-F** and its hydrodefluorinated analogue **2-H** have been synthesized and characterized using multinuclear NMR spectroscopy and single crystal X-ray diffraction. This transformation illustrates a rare and conceptually rich example of multi-step C–F and C–H bond making and breaking mediated by Rh/B cooperativity. These results not only elucidate an unusual reaction manifold of fluorinated organoboranes and a ubiquitous diolefin precursor but also highlight the broader potential of B–Rh cooperation in enabling multi-step synthesis of an emergent main-group heterocycle class.

The authors are grateful to Western University, the Council of Ontario Universities for a John C. Polanyi award to M. W. D., the Canadian Foundation for Innovation (LOF-212442), the Natural Sciences and Engineering Research Council of Canada

(Discovery Grant, RGPIN-2020-04480 (M. W. D.), Discovery Launch Supplement, DGECR-2020-00183), and graduate award (CGS-D/NSERC Vanier to J. A. Z.), and the Ontario Government (OGS award to E. J. A.) for funding. The calculations reported in this manuscript were performed using the ARCHIE-WeSt High-Performance Computer, hosted at the University of Strathclyde (archie-west.ac.uk); D. J. N. thanks J. Buzzard, Dr K. Karina-Ossowska, and Dr R. Martin for their assistance with this facility.

Conflicts of interest

There are no conflicts to declare.

Data availability

The data supporting this article have been included as part of the supplementary information (SI). Supplementary information: experimental procedures, spectroscopic data, computational details, crystallographic details, and additional references. See DOI: https://doi.org/10.1039/d6cc00158k. In addition, computational data underpinning this work can be downloaded from the ioChem-BD instance hosted at the Barcelona Supercomputing Centre: https://doi.org/10.19061/iochem-bd-6-620.

CCDC 2494566 (**2-F**/**2-H**) contains the supplementary crystallographic data for this paper.[45]

References

1 C. Gao and S. A. Blum, *Trends Chem.*, 2021, **3**, 645–659.
2 A. Amin, T. Qadir, P. K. Sharma, I. Jeelani and H. Abe, *Open Med. Chem. J.*, 2022, e187410452209010.
3 N. Matsumi, K. Naka and Y. Chujo, *J. Am. Chem. Soc.*, 1998, **120**, 5112–5113.
4 X. Su, T. A. Bartholome, J. R. Tidwell, A. Pujol, S. Yruegas, J. J. Martinez and C. D. Martin, *Chem. Rev.*, 2021, **121**, 4147–4192.
5 W. Schacht and D. Kaufmann, *Angew. Chem., Int. Ed. Engl.*, 1987, **26**, 665–666.
6 (*a*) A. Y. Houghton, V. A. Karttunen, W. E. Piers and H. M. Tuononen, *Chem. Commun.*, 2014, **50**, 1295–1298; (*b*) A. Y. Houghton, J. Hurmalainen, A. Mansikkamäki, W. E. Piers and H. M. Tuononen, *Nat. Chem.*, 2014, **6**, 983–988.
7 M.-A. Légaré, C. Pranckevicius and H. Braunschweig, *Chem. Rev.*, 2019, **119**, 8231–8261.
8 N. Wieprecht, I. Krummenacher, L. Wüst, M. Michel, S. Fuchs, S. Nees, M. Härterich and H. Braunschweig, *Chem. Sci.*, 2024, **15**, 12496–12501.
9 N. Wieprecht, I. Krummenacher, L. Wüst, M. Michel, M. Neder, A. Häfner, J. Karg and H. Braunschweig, *Chem. Sci.*, 2026, **17**, 2772–2780.
10 C. D. Entwistle and T. B. Marder, *Angew. Chem., Int. Ed.*, 2002, **41**, 2927–2931.
11 F. Jäkle, *Chem. Rev.*, 2010, **110**, 3985–4022.
12 L. Ji, S. Griesbeck and T. B. Marder, *Chem. Sci.*, 2017, **8**, 846–863.
13 P. A. Chase, W. E. Piers and B. O. Patrick, *J. Am. Chem. Soc.*, 2000, **122**, 12911–12912.
14 S. Bontemps, G. Bouhadir, K. Miqueu and D. Bourissou, *J. Am. Chem. Soc.*, 2006, **128**, 12056–12057.
15 L. A. Essex, J. W. Taylor and W. H. Harman, *Tetrahedron*, 2019, **75**, 2255–2260.
16 H. Braunschweig, I. Krummenacher and J. Wahler, *Advances in Organometallic Chemistry*, Elsevier, 2013, vol. 61, pp. 1–53.
17 G.-E. Herberich, B. Buller, B. Hessner and W. Os, *J. Organomet. Chem.*, 1980, **195**, 253–259.
18 G. J. Pindado, S. J. Lancaster, M. Thornton-Pett and M. Bochmann, *J. Am. Chem. Soc.*, 1998, **120**, 6816–6817.
19 S. Alvarez, *Dalton Trans.*, 2013, **42**, 8617.
20 B. Cordero, V. Gómez, A. E. Platero-Prats, M. Revés, J. Echeverría, E. Cremades, F. Barragán and S. Alvarez, *Dalton Trans.*, 2008, 2832.
21 D. A. Loginov, D. V. Muratov, P. V. Petrovskii, Z. A. Starikova, M. Corsini, F. Laschi, F. De Biani Fabrizi, P. Zanello and A. R. Kudinov, *Eur. J. Inorg. Chem.*, 2005, 1737–1746.
22 D. A. Loginov, D. V. Muratov, D. S. Perekalin, Z. A. Starikova, E. A. Petrovskaya, E. I. Gutsul and A. R. Kudinov, *Inorg. Chim. Acta*, 2008, **361**, 1715–1721.
23 G. E. Herberich, W. Boveleth, B. Hessner, M. Hostalek, D. P. J. Kijffer and M. Negele, *J. Organomet. Chem.*, 1987, **319**, 311–326.
24 M. K. Whittlesey and E. Peris, *ACS Catal.*, 2014, **4**, 3152–3159.
25 M. F. Kuehnel, D. Lentz and T. Braun, *Angew. Chem., Int. Ed.*, 2013, **52**, 3328–3348.
26 A. G. Massey and A. J. Park, *J. Organomet. Chem.*, 1966, **5**, 218–225.
27 M. Bursch, H. Neugebauer, S. Ehlert and S. Grimme, *J. Chem. Phys.*, 2022, **156**, 134105.
28 E. Caldeweyher, S. Ehlert, A. Hansen, H. Neugebauer, S. Spicher, C. Bannwarth and S. Grimme, *J. Chem. Phys.*, 2019, **150**, 154122.
29 J. Zheng, X. Xu and D. G. Truhlar, *Theor. Chem. Acc.*, 2011, **128**, 295–305.
30 A. V. Marenich, C. J. Cramer and D. G. Truhlar, *J. Phys. Chem. B*, 2009, **113**, 6378–6396.
31 S. Grimme, A. Hansen, S. Ehlert and J.-M. Mewes, *J. Chem. Phys.*, 2021, **154**, 064103.
32 F. Neese, *WIREs Comput. Mol. Sci.*, 2012, **2**, 73–78.
33 F. Neese, *WIREs Comput. Mol. Sci.*, 2022, **12**, e1606.
34 J. N. Harvey, F. Himo, F. Maseras and L. Perrin, *ACS Catal.*, 2019, **9**, 6803–6813.
35 C. Y. Legault, *CYLview20*. Université de Sherbrooke, 2020, Http://Www.Cylview.Org (https://Http://Www.Cylview.Org).
36 E. D. Glendening, J. K. Badenhoop, A. E. Reed, J. E. Carpenter, J. A. Bohmann, C. M. Morales, P. Karafiloglou, C. R. Landis and F. Weinhold, *NBO 7.0.*, Theoretical Chemistry Institute, University of Wisconsin, Madison, WI, 2018.
37 *Chemcraft - graphical software for visualization of quantum chemistry computations. Version 1.8, build 682*. https://www.chemcraftprog.com.
38 A. Iannetelli, G. Tizzard, S. J. Coles and G. R. Owen, *Inorg. Chem.*, 2018, **57**, 446–456.
39 M. Sajid, A. Lawzer, W. Dong, C. Rosorius, W. Sander, B. Schirmer, S. Grimme, C. G. Daniliuc, G. Kehr and G. Erker, *J. Am. Chem. Soc.*, 2013, **135**, 18567–18574.
40 M. Sajid, G. Kehr, T. Wiegand, H. Eckert, C. Schwickert, R. Pöttgen, A. J. P. Cardenas, T. H. Warren, R. Fröhlich, C. G. Daniliuc and G. Erker, *J. Am. Chem. Soc.*, 2013, **135**, 8882–8895.
41 H. C. Brown and S. K. Gupta, *J. Am. Chem. Soc.*, 1975, **97**, 5249–5255.
42 I. Peuser, R. C. Neu, X. Zhao, M. Ulrich, B. Schirmer, J. A. Tannert, G. Kehr, R. Fröhlich, S. Grimme, G. Erker and D. W. Stephan, *Chem. – Eur. J.*, 2011, **17**, 9640–9650.
43 R. Taube, S. Wache and J. Sieler, *J. Organomet. Chem.*, 1993, **459**, 335–347.
44 Q. Long, J. Gao, N. Yan, P. Wang and M. Li, *Org. Chem. Front.*, 2021, **8**, 3332–3341.
45 CCDC 2494566: Experimental Crystal Structure Determination, 2026, DOI: 10.5517/ccdc.csd.cc2pqsw3.

